INL/CON-22-70699-Revision-0

Channel Rank Improvement in Urban Drone Corridors Using Passive Intelligent Reflectors

March 2023

Ender Ozturk, Chethan Kumar Anjinappa, Fatih Erden, Ismail Guvenc, Huaiyu Dai, Md Moin Uddin Chowdhury, Arupjyoti Bhuyan

Changing the World's Energy Future

INL is a U.S. Department of Energy National Laboratory operated by Battelle Energy Alliance, LLC

INL/CON-22-70699-Revision-0

Channel Rank Improvement in Urban Drone Corridors Using Passive Intelligent Reflectors

Ender Ozturk, Chethan Kumar Anjinappa, Fatih Erden, Ismail Guvenc, Huaiyu Dai, Md Moin Uddin Chowdhury, Arupjyoti Bhuyan

March 2023

Idaho National Laboratory
Idaho Falls, Idaho 83415

http://www.inl.gov

Prepared for the
U.S. Department of Energy
Under DOE Idaho Operations Office
Contract DE-AC07-05ID14517

Channel Rank Improvement in Urban Drone Corridors Using Passive Intelligent Reflectors

Ender Ozturk*, Chethan K. Anjinappa*, Fatih Erden*, Md Moin Uddin Chowdhury*,
Ismail Guvenc*, Huaiyu Dai*, and Arupjyoti Bhuyan‡
***Department of Electrical and Computer Engineering, NC State University, Raleigh, NC 27695**
†INL Wireless Security Institute, Idaho National Laboratory, Idaho Falls, ID
eozturk3@its.jnj.com, {canjina,ferden,mchowdh,iguvenc,hdai}@ncsu.edu, arupjyoti.bhuyan@inl.gov

***Abstract*— Multiple-input multiple-output (MIMO) techniques can help in scaling the achievable air-to-ground (A2G) channel capacity while communicating with drones. However, spatial multiplexing with drones suffers from rank-deficient channels due to the unobstructed line-of-sight (LoS), especially in millimeter-wave (mmWave) frequencies that use narrow beams. One possible solution is utilizing low-cost and low-complexity metamaterial-based intelligent reflecting surfaces (IRS) to enrich the multipath environment, taking into account that the drones are restricted to flying only within well-defined drone corridors. A hurdle with this solution is placing the IRSs optimally. In this study, we propose an approach for IRS placement with a goal to improve the spatial multiplexing gains, and hence, to maximize the average channel capacity in a predefined drone corridor. Our results at 6 GHz, 28 GHz, and 60 GHz show that the proposed approach increases the average rates for all frequency bands for a given drone corridor when compared with the environment with no IRSs present, and IRS-aided channels perform close to each other at sub-6 and mmWave bands.**

TABLE OF CONTENTS

1. INTRODUCTION

Millimeter-wave (mmWave) bands offer an abundant amount of free spectrum to be exploited for increasing the mobile broadband data rates in 5G networks and beyond. The trade-off is the higher path loss that dictates a larger number of base stations (BSs) to achieve a similar coverage performance with a sub-6 GHz wireless network. Particularly in an urban drone corridor [1, 2], BS deployments around the corridor [3] introduce dominant line-of-sight (LoS) paths throughout the aerial service area (ASA). This diminishes the spatial multiplexing gains for multiple-input multiple-output (MIMO) communication links with the drones. One way of enhancing the channel capacity via spatial multiplexing is by deploying reflectors with beam-steering and focusing functions. This will help create a favorable propagation environment by introducing new multipath components (MPCs) to the channel, hence, increasing the overall spatial diversity.

Optimal placement of BSs has been studied with several different performance criteria in the literature, such as cost, coverage, and capacity [4, 5]. The optimal placement of reflectors is also studied with similar motivations. In [6], authors maximize coverage area considering BSs and passive metallic reflectors (PMRs) in an outdoor urban setting, while [7] presents channel sounding results to explore coverage gains when using passive reflectors. Metallic reflectors do not have the capability to tilt the incident wave, but they only reflect towards the specular direction without focusing, which yields excess loss in comparison with metamaterial-based intelligent reflecting surfaces (IRSs) with beamforming capabilities [8]. The necessity to have a certain physical tilt angle also makes the PMRs less practical in an urban area due to cosmetic and logistic reasons. Optimal network design using IRSs is a relatively new topic in the literature [9]. In [10], optimum placement of IRSs is studied to eliminate the coverage holes in an urban area, which shows that properly deployed IRSs can fulfill the predefined coverage goals even with imperfect context information. In [11], IRS placement problem is formulated by considering their sizes and operating modes to increase the reliability of vehicle-to-everything (V2X) communications.

It is shown in [12] that a single IRS can improve the channel matrix rank to support spatial multiplexing; however, optimal placement of IRSs in scale remains unaddressed. In this work, we study the optimal placement of IRSs to maximize the average channel capacity in a drone corridor. In terms of drone corridor design, there are studies in the literature that explore optimum trajectory of a drone with existing BSs to keep the channel rate above some threshold, which could result in fluctuations throughout the route. In this work, we study how we can improve throughput on predefined drone routes by manipulating the propagation environment rather than changing the drone's trajectory. For a given set of candidate IRS locations, a BS, and a drone corridor (defined in terms of ASAs), and assuming MIMO communication, we assign IRSs to aerial surface areas such that the average downlink (DL) capacity in the corridor is maximized. In our work, we used path loss models given in the literature to calculate the rates. Subsequently, we formulated and solved an optimization problem to find optimal locations

978-1-6654-9032-0/23/$31.00 ©2023 IEEE

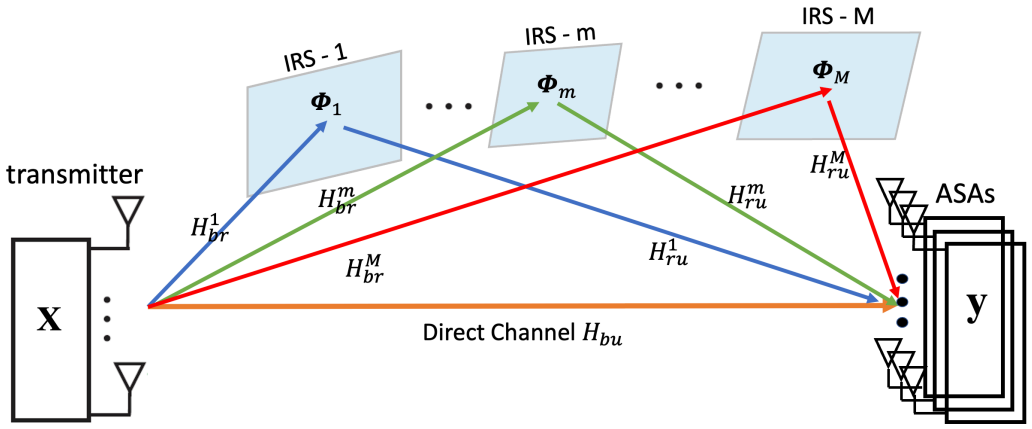

Figure 1. System model: introducing multiple IRSs in the environment can improve the spatial multiplexing gains at given locations in a drone corridor. A downlink scenario from a BS to UAVs is considered in the paper. Similar analysis can be done for uplink.

of passive IRSs in a given candidate set, to maximize the average capacity in the ASAs (drone corridor), which to our knowledge have not been explored in the literature.

The rest of this paper is organized as follows. The system model is introduced in Section 2, and the proposed optimization process is explained in Section 3. Then the numerical results are shared in Section 4, and the paper is concluded in Section 5.

2. System Model

We consider an IRS-assisted MIMO system as in Figure 1, where the users are defined to be within equally spaced ASAs that constitutes a drone corridor. In this study, only passive reflectors are considered that do not require any dynamic beamforming and hence have cost and power-efficiency advantages. In this paper, aligned with some other existing literature [13, 14], we still refer to such reflectors as IRSs, as they are designed to have unique reflection characteristics using meta-surfaces. Consequently, in this design, a single IRS is assumed to serve only a single ASA. Let the channel be an $N_{\text{rx}} \times N_{\text{tx}}$ MIMO channel. The total number of ASAs, and IRSs and unit cells on the m^{th} IRS are given as ξ, ψ, and N_m, respectively. Channel matrix can be decomposed into two components, namely, line-of-sight (LoS) component, and guided reflection component.

LoS Transmission

The received signal is the superposition of LoS component and the guided reflection component in this model. The received LoS signal $\mathbf{y}_{\text{LoS}} \in \mathbb{C}^{\mathbb{N}_{\text{rx}} \times \mathbb{K}}$ is defined as $\mathbf{y}_{\text{LoS}} = \mathbf{H}_{\text{bu}}\mathbf{V}\mathbf{x} + \mathbf{n}$, where $\mathbf{x} \in \mathbb{C}^{\mathbb{N}_{\text{tx}} \times \mathbb{K}}$ is the transmitted signal, $\mathbf{V} \in \mathbb{C}^{\mathbb{N}_{\text{tx}} \times \mathbb{N}_{\text{tx}}}$ is the precoding matrix at the BS, $\mathbf{n} \sim \mathcal{CN}(,\boldsymbol{\sigma}\mathbf{I})$ is the complex additive white Gaussian noise (AWGN), and $\mathbf{H}_{\text{bu}} \in \mathbb{C}^{\mathbb{N}_{\text{rx}} \times \mathbb{N}_{\text{tx}}}$ is the direct channel. The singular value decomposition of $\mathbf{H}_{\text{bu}}$ is equal to $\mathbf{U}\boldsymbol{\Lambda}\mathbf{V}^H$, where $\mathbf{U} \in \mathbb{C}^{\mathbb{N}_{\text{rx}} \times \mathbb{N}_{\text{rx}}}$ and $\mathbf{V}$ are unitary matrices by definition, and $\boldsymbol{\Lambda} \in \mathbb{R}_+^{\mathbb{N}_{\text{rx}} \times \mathbb{N}_{\text{tx}}}$ is the diagonal singular value matrix.

Given these, the received signal at the user side can be rewritten as $\mathbf{U}^H\mathbf{y}_{\text{LoS}} = \mathbf{U}^H\mathbf{H}_{\text{bu}}\mathbf{V}\mathbf{x} + \mathbf{U}^H\mathbf{n}$.

A single entry of the channel matrix, $\mathbf{H}_{\text{bu}}$, is given by $\sqrt{\beta^{t,u}}e^{j2\pi\frac{d_{t,u}}{\lambda_c}}$, where $\beta^{t,u}$ is the free-space path loss component, $d^{t,u}$ is the distance between the t^{th} transmitter antenna and the u^{th} receiver antenna, and λ_c is the wavelength. We assume $\beta^{t,u}$ to be approximately equal for all (t,u) pairs in the far field. In this LoS scenario, $\mathbf{H}_{\text{bu}}$ has a single non-zero singular value, λ_d, hence, as given in [15], the channel capacity in bit/s/Hz is

$$R_{\text{LoS}} = \log_2\left(1 + \frac{P_{\text{tot}}\lambda_d^2}{\sigma^2}\right), \tag{1}$$

where P_{tot} is the total radiated power and σ^2 is the noise power.

Guided Reflection Component

When IRSs are used, new received components enrich the multipath environment and enable additional data streams to increase the capacity. Let $\mathbf{H}_{\text{br}}^m \in \mathbb{C}^{\mathbb{N}_{\mathbb{>}} \times \mathbb{N}_{\text{tx}}}$ be the channel between the transmit antennas and the m^{th} IRS. A single normalized matrix element that associates the i^{th} cell of the m^{th} reflector to the t^{th} transmit antenna $\hat{h}_{\text{br}}^{t,m,i}$ is expressed as

$$\hat{h}_{\text{br}}^{t,m,i} = e^{j2\pi d_{\text{br}}^{t,m,i}\frac{1}{\lambda_c}}, \tag{2}$$

where $d_{\text{br}}^{t,m,i}$ is the distance between the transmit antenna and the unit cell under consideration.

Now let $\mathbf{H}_{\text{ru}}^m \in \mathbb{C}^{\mathbb{N}_{\text{rx}} \times \mathbb{N}_{\mathbb{>}}}$ be the channel between the m^{th} IRS and the receive antennas. Similarly, a single normalized matrix element that associates the u^{th} receive antenna to i^{th} cell of the m^{th} reflector $\hat{h}_{\text{ru}}^{u,m,i}$ is expressed as $\hat{h}_{\text{ru}}^{u,m,i} = e^{j2\pi\frac{d_{\text{ru}}^{u,m,i}}{\lambda_c}}$, where $d_{\text{ru}}^{u,m,i}$ is the distance between the receive antenna and

the unit cell under consideration. Given these definitions, the channel equation for the guided reflection scenario becomes $\mathbf{y}_u = \mathbf{H}_c \mathbf{V}_u \mathbf{x} + \mathbf{n}$, where $\mathbf{V}_u$ is the precoding matrix at the BS, and $\mathbf{H}_c$ is the compound channel matrix, which can be expressed in terms of the set $\mathcal{L}$ that contains the indexes of IRSs that are dedicated to serve a particular ASA. It can be expressed as:

$$\mathbf{H}_c = \left(\sum_{m \in \mathcal{L}} \mathbf{H}_{ru}^m \mathbf{\Phi}^m \mathbf{H}_{br}^m \right) + \mathbf{H}_{bu}, \tag{3}$$

where $\mathbf{\Phi}^m = \alpha_m \text{diag}(e^{j\phi_1^m}, e^{j\phi_2^m}, \ldots, e^{j\phi_{N_m}^m})$ is the diagonal phase contribution matrix of the m^{th} reflector, and α_m is the reflection loss. The expression in parenthesis in (3), even though not stated explicitly, includes the free-space path loss from the transmitter to the receiver via the m^{th} reflector, β_c^m. In this study, the path loss model in [16] is used, which can be modified for a square shape reflector as

$$\beta_c^m = \frac{G_t G_u}{(4\pi)^2} \left(\frac{N_m d_\lambda^{m2}}{d_{\text{br}}^m d_{\text{ru}}^m} \right)^2 \cos^2(\phi_m^t), \tag{4}$$

where G_t and G_u are the antenna gains of the transmitter and the receiver, d_λ^m is the size of the unit cell of m^{th} reflector, and ϕ_m^t is the angle of incidence. The path loss expression includes only the incident angle but not the angle of departure. This is because that term vanishes as the size of the reflector gets smaller, i.e., whole IRS can be interpreted as an array of diffuse scatterers, where each unit cell is a scatterer with adjusted phase contribution to direct the beam to a specific direction. As a result of this assumption, there is no need to consider what exactly each individual phase contributions should be in this study as long as they are arranged properly to collimate the beam. Details could be found in [16] Section III.B.

Let the total number of non-zero singular values of the compound channel be S, where each singular value λ_s is a function of physical positions of all reflectors in $\mathcal{L}$ as well as their orientations, sizes, and phase contributions. These singular values can be calculated for a given setting by first calculating the necessary phase distribution matrix assuming that the reflected signal is directed to the receiver, then finding the channel matrix and performing singular value decomposition. For a given set of singular values, the total rate of the compound channel is given in [15] as

$$R_{\text{IRS}} = \sum_{s=1}^{S} \log_2 \left(1 + \frac{P_s \lambda_s^2}{\sigma^2} \right), \tag{5}$$

where P_s is the amount of power allocated for a specific data stream, and is defined using water filling algorithm given by $P_s = \left(\mu - \frac{\sigma^2}{\lambda_s^2} \right)^+$, where μ is chosen to satisfy the total power constraint, i.e., $\sum_s P_s = P_{\text{tot}}$.

3. Drone Corridor Reflector Placement

The goal of this study, building on the system model presented earlier, is to find the optimal locations of IRSs among a given set of candidate locations, in order to maximize the average channel rate at a specific drone corridor while considering certain design criteria (see Figure 2a). The drone corridor is represented by a sequence of uniformly spaced ASAs. Assigning an IRS to a specific ASA requires adjusting the IRS phase map such that the reflected signal from the IRS is directed towards that ASA. The optimization problem's design constraints include: 1) each ASA being served by a single IRS; 2) each IRS serving a single ASA; 3) constraint on the amount of energy that an IRS acquires; and 4) size limitation of IRSs subject to the far-field constraint. We will capture all these limitations by formulating the problem as a binary integer linear programming (BILP) problem.

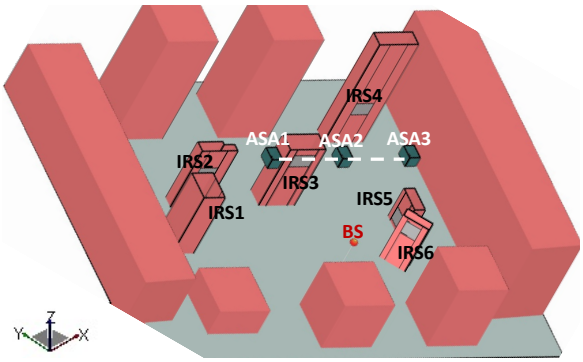

(a)

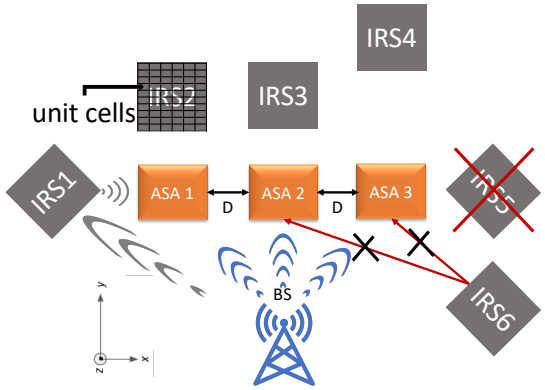

(b)

Figure 2. A sample scenario consisting of a single BS, 3 ASAs, and 6 IRSs: a) Illustration of the drone corridor with ASAs in an urban setting; b) IRS, ASA and BS relative locations with parameters introduced. IRS5 cannot serve any of the ASAs as the incident angle is above the required threshold. IRS6 cannot serve ASA2 and ASA3 due to limitation on the reflection angle.

The candidate IRS set should be created depending on the environment. For a given environment, the possible IRS locations should be expressed in terms of reflector center and 3D surface normal vector representing the boresight of the surface. The BS and the ASA locations should be defined before beginning the optimization process. A sample layout in 2D is given in Figure 2b.

The first step in the process is applying maximum incident angle limitation to create a feasible candidate IRS list for each ASA. The incident angle of the incoming ray from the transmitter on the IRS should be less than a threshold value, Φ_c^{i}. Intuitively, from (4), the amount of energy that can be steered by the IRS is proportional with the $\cos^2(\cdot)$ of the incident angle. In this regard, Φ_c^{i} is a design parameter to narrow down or broaden the candidate IRS list that can serve to a specific ASA. The initial universal set is reduced by eliminating IRSs that do not meet $\phi_m^{\mathrm{tx}} < \Phi_c^{\mathrm{i}}$ condition, where ϕ_m^{tx} is the angle of incidence on the m^{th} IRS.

On the reflection side, another limit should be applied, i.e., the departure angle of the outgoing ray from the IRS to the receiver should be less than another threshold value, Φ_c^{r}. This limitation is based on the physical optics approximations used to derive the path loss models. It is seen in Figure 2b that IRS5 cannot serve any ASA, because of its orientation, whereas IRS6 is dropped from ASA2 and ASA3 candidate IRS lists due to the same reason. Broadening the list may yield a higher average rate in the drone corridor as the optimization algorithm has a wider set of choices at the cost of increased computation time for finding optimal IRS-ASA assignments. The resulting set after applying these two conditions is expressed as:

$$\mathcal{L}_{\mathrm{i,r}}^{\prime\prime} \in \Big\{ (\S, , , \hat{\mathbf{n}}) \quad | \forall m \in [M], \quad \forall \phi_m^{\mathrm{tx}} < \Phi_c^{\mathrm{i}}, \forall \phi_m^{\mathrm{rx}} < \Phi_c^{\mathrm{r}} \Big\}, \tag{6}$$

where $[M]$ represents the set of candidate IRSs. We will refer this set as $\mathcal{L}^{\prime}$ for simplicity. The optimization problem for finding the IRS-ASA matches can then be formulated as:

$$\begin{aligned}
\max_{\alpha_u^\mu} \quad & \frac{1}{\xi} \sum_u \sum_\mu \alpha_u^\mu \mathrm{R}_{u,\mu} \\
\text{s.t.} \quad c_0: \quad & \mu \subseteq [M^U], \\
c_1: \quad & \alpha_u^m \in \{0,1\} \quad \forall m \in [M], \forall u \in [U], \\
c_2: \quad & \sum_{u=1}^{U} \alpha_u^m \leq 1, \quad \forall m \in \mathcal{L}^{\mathrm{m,\,u}}, \\
c_3: \quad & \sum_{\mathcal{L}^{\mathrm{m,\,u}}} \alpha_u^m \leq s_{\max}, \quad \forall u \in [U], \\
c_4: \quad & N_m^u = \min\left(\left\lfloor \frac{d_{\mathrm{ru}}^m}{4 d_\lambda^m} \right\rfloor, N_{\max} \right) \forall m \in \mathcal{L}^{\mathrm{m,\,u}}, \forall \in [\mathcal{U}].
\end{aligned} \tag{7}$$

Notation used above is explained further below while describing the objective function and the constraints.

- ***Objective Function:*** The objective of the process is to find the IRS-ASA pairs that maximizes the average rates throughout the drone corridor, where ξ is the cardinality of ASA set, $[U]$, and $\mathrm{R}_{u,\mu}$ is the channel rate from (5), achieved when all the IRSs in subset-μ serve the u^{th} ASA.
- ***Constraint 0:*** μ represents different combinations of IRSs that are chosen to serve an ASA, and it should be a subset of the universal IRS candidate set, $[M^U]$. $[M^U]$ includes all combinations of IRS selections, i.e., if $[M]$ has ζ elements, $[M^U]$ will have $2^\zeta - 1$ elements excluding the empty set.
- ***Constraint 1:*** $\alpha_u^m \in \{0,1\}$ is 1 when m^{th} reflector is assigned to serve u^{th} ASA, and 0 otherwise.
- ***Constraint 2:*** Any IRS can be assigned only to a single ASA as we consider passive IRSs. Passive IRSs are affordable, and less complicated as no control mechanism is required. The sum of α_u^m over u hence should not exceed 1.
- ***Constraint 3:*** The number of IRSs that are assigned to a certain ASA is limited by $s_{\max}$. In theory, it is possible to increase the capacity of the direct channel by $s_{\max}$ folds or even further with high gains if $s_{\max} \leq \min(N_{\mathrm{tx}}, N_{\mathrm{rx}})$. A higher $s_{\max}$ yields increased computational complexity; however, this is not a concern as the optimization process runs offline and the IRSs are placed only once. The variable $s_{\max}$ is used to limit the number of IRSs per ASA, as gains are expected to be limited with larger number of ASAs per IRS due to geometrical and path loss constraints.
- ***Constraint 4:*** Even though the high path loss in mmWave frequencies impel the designers to deploy larger reflectors for higher reflection gains, far-field approximations constitute a natural barrier. In a specific design, the size of an IRS can be the minimum of: 1) the maximum size that is feasible due to physical constraints, and 2) the size of the reflector that the ASA served by that IRS resides at the border of the IRS's Fresnel zone, which is $4a^2/\lambda_c$, where a is the edge dimension of a square reflector. This limit has been expressed in terms of maximum allowed unit cells, $N_{\max}$, assuming a square shaped reflector in (7).

The BILP problem given in (7) is an NP-hard resource allocation problem and can be solved using GUROBIPY library in Python that aims to search for the global optimum.

4. NUMERICAL RESULTS

In this section, we provide simulation results using the proposed BILP-based approach in (7), to find optimum IRS locations for a given BS, three ASA points, and six candidate reflector locations. Simulation parameters are given in Figure 2b and Table 1. The IRS locations are chosen to have heights lower than the ASAs and the BS in compliance with an urban setting where billboards or walls of the buildings can be utilized as reflectors. We consider a 2×2 MIMO scheme and three different central frequencies, i.e., $f_{\mathrm{c}} =$ 6, 28, 60 GHz, and three different ASA separations, i.e., $D = 20$, 30, 40 m. The expression given in (5) are used for the rate calculations. We will explain our findings in subsequent subsections.

Frequency Dependency of ASA-IRS Association

First, the corresponding rates are calculated for all IRS-ASA pairs assuming that the reflector's phase distribution is adjusted to serve that specific ASA, and a database is created. Then the BILP algorithm defines the IRS-ASA matches assuring the maximum average rate over the ASA. The optimized IRS-ASA pairs that maximize the average rates in the drone corridor are shown in Table II together with the corresponding unit cell counts. We observe that the best

Table 1. Simulation parameters.

Parameter	Value
Center frequencies	$f_c = 6, 28, 60$ GHz
IRS element spacing	$d_\lambda^m = 0.25\ \lambda$
BS center location	(0,0,20) m
ASAs center locations	$(-D,20,30)$, (0,20,30), $(D,20,30)$ m
ASA separation	$D = 20, 30, 40$ m
IRS Locations	(-20,20,30) (-25,30,10) (0,30,10) (25,50,10) (30,20,1) (25,10,10) m
Receiver noise power	$\sigma^2 = -94$ dBm
Total power	$P_{\text{tot}} = 10$ dBm
Antenna gains	$G_{\text{tx}} = G_{\text{rx}} = 3$ dBi
Max serving IRS	$s_{\max} = 1$
Max incident/reflection angles	$\Phi_c^i = \Phi_c^r = 80$ deg
Max allowed reflector size	0.25 m^2

Table 2. Optimum IRS-ASA matches and unit cell counts ($D =$ 20 m).

Match (Cells)	6 GHz	28 GHz	60 GHz
ASA 1	IRS 1 (1600)	IRS 4 (21316)	IRS 6 (40000)
ASA 2	IRS 2 (1600)	IRS 1 (13456)	IRS 1 (28900)
ASA 3	IRS 4 (1600)	IRS 2 (18769)	IRS 2 (40000)

IRS-ASA matches change with frequency, since the path loss behaviour and the Fresnel zones of the IRSs are frequency dependent. In cases that the IRS sizes are defined to be the maximum allowed size of 0.25 m^2, the number of unit cells are capped with the corresponding count (1600 for 6 GHz and 40,000 for 60 GHz).

In addition, IRS 4 is the farthest reflector to all ASAs as shown in Figure 2b, and despite the high path loss, it qualifies to serve an ASA for 6 GHz and 28 GHz bands with the help of additional gain that comes with focusing and angular separation. However, path loss becomes too high at 60 GHz and hence IRS 4 no longer provides adequate rates. Even though IRS 3 is the closest to all three ASAs, due to the lack of angular separation of received rays by ASAs when IRS 3 is in use, channels with IRS 3 give quite low rates [15]. Another observation for 20 m separation is that, IRS 1 is matched with ASA 1 in 6 GHz (the closest), however, IRS 4 is matched with ASA 1 in 28 GHz (the farthest). The reason for that is, when the frequency increases, the Fresnel zone of the IRS also widens, and consequently, being close to the receiver becomes no longer advantageous as the reflector size needs to be smaller to keep the ASA outside of the near field.

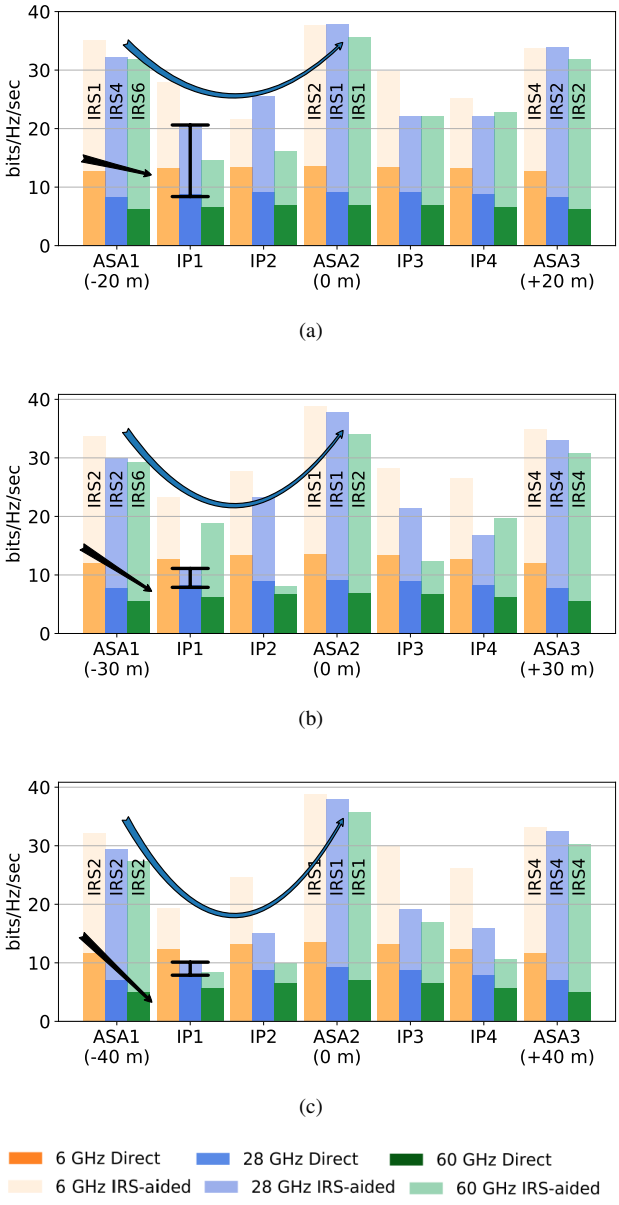

Figure 3. Achieved channel rates for different ASA separations: a) $D = 20$ m, b) $D = 30$ m, c) $D = 40$ m. Direct channel and IRS-aided channel rates, and the associated IRS are given within the same bar for different frequency bands. As the separation increases, interim point (IP) rates reduce more.

Effect of IRSs on Path Loss

The achieved channel rates are given for three different frequency bands at three ASAs in Figure 3, together with the direct channel rates. Simulation results show that IRS-aided channels have significantly higher rates; for example, the rate for ASA1 at 20 m ASA separation increases from 12.8 bit/s/Hz to 35.2 bit/s/Hz at 6 GHz.

Also note that as the frequency increases, all rates decrease due to increased path loss; however, the IRS-aided channels

suffer less than direct channels. Maximized average rates, which are calculated by averaging the achieved rates over the three ASAs, with $D = 20$ m ASA separation for $f = 6$, 28, 60 GHz bands are calculated as 35.5, 34.7, 33.1 bit/s/Hz, respectively, whereas, direct channel rates are found to be 13.1, 8.6, 6.5 bit/s/Hz. The IRS-aided channels rates are close to each other even when the frequency increases. The first reason for this behavior is that, a maximum allowed reflector size is used in the simulations, which is given in Table 1 as 0.25 m^2. For 6 GHz band, this IRS size constraint predominates the far-field constraint, and hence all the IRSs have this maximum allowed size even though a larger IRS would ideally be required. In case that this cap is removed for 6 GHz frequency band, only the far-field constraint remains, and subsequently, best IRS-ASA matches change after the optimization process. With this new assumption, instead of rates and matchings in Figure 3, we would see ASA 1 matches with IRS 6, ASA 2 matches with IRS 1, and ASA 3 matches with IRS 2. Maximum average rate throughout the drone corridor becomes 39.7 bit/s/Hz with average area of 0.56 m^2.

The underlying second reason can be better explained by rewriting (4) in terms of the reflector area, A, which is defined as $\min(0.25\text{m}^2, \lambda d_{\text{ru}}/4)$ where the second term represents the surface area that ensures the ASA outside of the IRS's Fresnel zone. For mmWave frequencies, the far-field constraint predominates the reflector size constraint: $\beta_c \propto \left(\frac{A}{d_{\text{br}} d_{\text{ru}}}\right)^2 \propto \left(\frac{\lambda}{4 d_{\text{br}}}\right)^2$. The reflector index, m, and some additional terms are omitted for lucidity. This expression shows that the introduction of an IRS compensates for the effect of the path loss that comes from the distance between the IRS and the ASA, hence, the increased channel rates. Note that, one component of the compound channel, given in (3), is the direct channel and the direct channel suffers from the path loss as usual.

A less influential reason for the channel rates to be close to each other is that, as the frequency band changes, the best IRS-ASA matches also change, which yields to less worse channel rates, i.e., for $D = 20$ m separation, in case that the same best IRS-ASA matches of the 28 GHz band are used for the 60 GHz band, the maximum average rate would be 32.5 bit/s/Hz instead of 33.1 bit/s/Hz.

Effect of ASA Separation on MIMO Rates

Fig 3 shows that, with increased separation between ASAs, the rates calculated for ASA 1 and ASA 3 decrease due to the increased distances and due to the fact that changing the ASA locations eliminates some IRSs from the ASA candidate lists or some IRSs become less useful (e.g. at $D = 30$ m, IRS 1 is no longer an option for ASA 1, and at $D = 40$ m, ASA 3 is further away from IRS 1 and IRS 2, and IRS 4 becomes a better option). Hence, overall average achieved rates reduce.

The IRSs are optimized for serving ASAs, however one still expects the reflectors to perform well in between the ASAs, as long as the separation is not high. In this respect, we also studied the performance in the points in between the ASAs in Figure 3, the interim points, when the IRSs are optimized for the ASAs, for different separations of the ASAs. We defined the interim points for each segment (i.e., ASA1-ASA2 segment) as the two points that divides the segment into three equal subsegments. The same scenario described in Figure 2b is assumed. In these simulations, the location of ASA 2 is kept fixed and, ASA 1 and ASA 3 are moved further away. Separation distances of $D = 20, 30, 40$ m are investigated. In general, the calculated rates in Figure 3 are closer to the rates at the nearest ASA, however, at some instances, the rates drop significantly. The reason for that is, at those specific points, interim points coincide with the reflector pattern nulls, and consequently, achieved rates decrease drastically. Note that there is a trade-off between the separation distance and average achievable rate throughout the corridor where the interim points are included. One should take the separation into account while designing a drone corridor in case there is a minimum rate requirement throughout the corridor.

5. Conclusion and Future Work

In this paper, we studied the placement problem of IRSs to maximize the average channel capacity throughout predefined service areas. For a given BS, a set of ASAs (representing a drone corridor), and a set of candidate reflector positions, the proposed BILP-based optimization approach associates the IRSs with the ASAs so that the average rate with spatial multiplexing is maximized in the drone corridor. Our simulation results show that the average capacity of the channel in a 2×2 MIMO setting increased from 13.1 to 35.5 bit/s/Hz at 6 GHz, from 8.6 to 34.3 bit/s/Hz at 28 GHz, and from 6.5 to 33.1 bit/s/Hz at 60 GHz when the IRSs are used. In future, we plan to extend this work exploring different schemes for defining candidate reflector set, evaluate the performance in other bands such as the E-Band and subterahertz bands, study the impact of shadowing and fading on the achievable rate and bit error rate, consider performance dependence to relative positions of reflectors to users/BSs, and explore multi-reflection and multi-user scenarios.

6. Acknowledgements

This work is supported in part by the INL LDRD Program under the Contract DEAC07-05ID14517, and by ARO under Grant W911NF-16-1-0448.

References

[1] FAA, "Urban Air Mobility (UAM) Concept of Operations," Technical Report, June 2020. [Online]. Available: https://nari.arc.nasa.gov/sites/default/files/attachments/UAM_ConOps_v1.0.pdf

[2] A. Bhuyan, I. Guvenc, H. Dai, Y. Yapici, A. Rahmati, and S. J. Maeng, "Secure mmWave cellular network for drone communication," in *Proc. IEEE Veh. Techn.*

Conf., Apr. 2019, pp. 1–5.

[3] S. Singh, U. Bhattacherjee, E. Ozturk, I. Guvenc, H. Dai, M. L. Sichitiu, and A. Bhuyan, "Placement of mmWave base stations for serving urban drone corridors," in *Proc. IEEE Veh. Techn. Conf.*, Apr. 2021, pp. 1–5.

[4] I. Mavromatis, A. Tassi, R. J. Piechocki, and A. Nix, "Efficient millimeter-wave infrastructure placement for city-scale ITS," in *Proc. IEEE Veh. Techn. Conf.*, Kuala Lumpur, Malaysia, Apr. 2019, pp. 1–5.

[5] F. Erden, C. K. Anjinappa, E. Ozturk, and I. Guvenc, "Outdoor mmWave base station placement: A multi-armed bandit learning approach," *arXiv preprint arXiv:2003.03494*, 2020.

[6] C. K. Anjinappa, F. Erden, and I. Güvenç, "Base station and passive reflectors placement for urban mmwave networks," *IEEE Trans. Veh. Technol.*, vol. 70, no. 4, pp. 3525–3539, 2021.

[7] W. Khawaja, O. Ozdemir, Y. Yapici, F. Erden, and I. Guvenc, "Coverage enhancement for NLOS mmWave links using passive reflectors," *IEEE Open J. Commun. Soc.*, vol. 1, pp. 263–281, Feb. 2020.

[8] S. Kutty and D. Sen, "Beamforming for millimeter wave communications: An inclusive survey," *IEEE Commun. Surveys Tuts.*, vol. 18, no. 2, pp. 949–973, Dec. 2015.

[9] S. Gong, X. Lu, D. T. Hoang, D. Niyato, L. Shu, D. I. Kim, and Y. C. Liang, "Toward smart wireless communications via intelligent reflecting surfaces: A contemporary survey," *IEEE Commun. Surveys Tuts.*, vol. 22, no. 4, pp. 2283–2314, June 2020.

[10] K. Heimann, A. Marsch, B. Sliwa, and C. Wietfeld, "Reflecting surfaces for beyond line-of-sight coverage in millimeter wave vehicular networks," in *Proc. IEEE Vehic. Netw. Conf. (VNC)*, 2020, pp. 1–4.

[11] Y. U. Ozcan, O. Ozdemir, and G. K. Kurt, "Reconfigurable intelligent surfaces for the connectivity of autonomous vehicles," *IEEE Trans. Veh. Technol.*, vol. 70, no. 3, pp. 2508–2513, 2021.

[12] O. Özdogan, E. Björnson, and E. G. Larsson, "Using Intelligent Reflecting Surfaces for Rank Improvement in MIMO Communications," in *Proc. IEEE Int. Conf. Acoustics, Speech, Sig. Process. (ICASSP)*, Barcelona, Spain, May 2020, pp. 9160–9164.

[13] J. Lyu and R. Zhang, "Hybrid active/passive wireless network aided by intelligent reflecting surface: System modeling and performance analysis," *IEEE Trans. Wireless Commun.*, pp. 1–1, 2021.

[14] M. Najafi, V. Jamali, R. Schober, and H. V. Poor, "Physics-based modeling and scalable optimization of large intelligent reflecting surfaces," *IEEE Trans. Commun.*, vol. 69, no. 4, pp. 2673–2691, 2021.

[15] P. V. David Tse, *Fundamentals of Wireless Communication*. Cambridge University Press, 2005.

[16] O. Özdogan, E. Björnson, and E. G. Larsson, "Intelligent reflecting surfaces: Physics, propagation, and pathloss modeling," *IEEE Wireless Commun. Lett.*, vol. 9, no. 5, pp. 581–585, May 2020.

BIOGRAPHY

Ender Ozturk received his B.S. and M.S. degrees from Bilkent University, Ankara, Turkey, in 2005 and 2008, respectively, and the Ph.D. degree from Hacettepe University, Ankara, Turkey, in 2018, all in electrical and electronics engineering. He held different positions in industry as an engineer, senior engineer and team leader. He worked as a Postdoctoral Research Scholar at North Carolina State University until 2021, and currently working at J&J.

Chethan K. Anjinappa received his BE degree in Electronics and Communication Engineering from Sri Jayachamarajendra College of Engineering, Mysuru, India, in 2012 and ME degree in Signal Processing from Indian Institute of Science (IISc), Bengaluru, India in 2016. He then worked as a Project Associate in Signal Processing for Communications lab, IISc during 2016-2017. He is currently pursuing a Ph.D. degree in Electrical Engineering at North Carolina State University.

Fatih Erden received the B.S. and M.S. degrees from Bilkent University, Ankara, Turkey, in 2007 and 2009, respectively, and the Ph.D. degree from Hacettepe University, Ankara, Turkey, in 2015, all in electrical and electronics engineering. From 2015 to 2016, he was an Assistant Professor with the Department of Electrical and Electronics Engineering, Atilim University, Ankara, Turkey. From 2016 to 2018, he was with the Signal Processing Group, Bilkent University, Ankara, Turkey, as a Postdoctoral Researcher. Since 2018, he has been a Research Associate with the Department of Electrical and Computer Engineering, North Carolina State University. His research interests include signal and image processing, machine learning, time-series analysis, mmWave communications, and UAVs.

Md Moin Uddin Chowdhury received his BS degree in Electrical and Electronic Engineering from Bangladesh University of Engineering and Technology in 2014 and MS in Electrical Engineering from North Carolina State University in 2020. He is currently pursuing PhD in the same institute where he is currently working on integrating drones into cellular networks.

Ismail Güvenc (F'21) received the Ph.D. degree in electrical engineering from the University of South Florida in 2006. He was with the Mitsubishi Electric Research Labs in 2005, with DOCOMO Innovations from 2006 to 2012, and with Florida International University, from 2012 to 2016. From 2016 to 2020, he has been an Associate Professor, and since 2020, he has been a Professor, with the Department of Electrical and Computer Engineering of North Carolina State University. He has published more than 300 conference/journal articles and book chapters, and several standardization contributions. He coauthored/co-edited four books and he is an inventor/co-inventor of some 30 U.S. patents. His recent research interests include 5G wireless systems, communications and networking with drones, and heterogeneous wireless networks.

Dr. Güvenç is a Senior Member of the National Academy of Inventors. He was a recipient of the USF Outstanding Dissertation Award in 2006, the Ralph E. Powe Junior Faculty Enhancement Award in 2014, the NSF CAREER Award in 2015, the FIU College of Engineering Faculty Research Award in 2016, and the NCSU ECE R. Ray Bennett Faculty Fellow Award in 2019. He has served as an Editor for the IEEE Communications Letters from 2010 to 2015 and the IEEE Wireless Communications Letters from 2011 to 2016. He has been serving as an Editor for the IEEE Transactions on Wireless Communications since 2016, and for IEEE Transactions on Communications since 2020. He has served as a guest editor for several other journals.

Huaiyu Dai (F'17) received the B.E. and M.S. degrees in electrical engineering from Tsinghua University, Beijing, China, in 1996 and 1998, respectively, and the Ph.D. degree in electrical engineering from Princeton University, Princeton, NJ in 2002. He was with Bell Labs, Lucent Technologies, Holmdel, NJ, in summer 2000, and with AT&T Labs-Research, Middletown, NJ, in summer 2001. He is currently a Professor of Electrical and Computer Engineering with NC State University, Raleigh. His research interests are in the general areas of communication systems and networks, advanced signal processing for digital communications, and communication theory and information theory. His current research focuses on networked information processing and crosslayer design in wireless networks, cognitive radio networks, network security, and associated information-theoretic and computation-theoretic analysis.

He has served as an editor of IEEE Transactions on Communications, IEEE Transactions on Signal Processing, and IEEE Transactions on Wireless Communications. Currently he is an Area Editor in charge of wireless communications for IEEE Transactions on Communications. He co-edited two special issues of EURASIP journals on distributed signal processing techniques for wireless sensor networks, and on multiuser information theory and related applications, respectively. He co-chaired the Signal Processing for Communications Symposium of IEEE Globecom 2013, the Communications Theory Symposium of IEEE ICC 2014, and the Wireless Communications Symposium of IEEE Globecom 2014. He was a co-recipient of best paper awards at 2010 IEEE International Conference on Mobile Ad-hoc and Sensor Systems (MASS 2010), 2016 IEEE INFOCOM BIGSECURITY Workshop, and 2017 IEEE International Conference on Communications (ICC 2017).

Arupjyoti (Arup) Bhuyan (SM'13) is a wireless researcher in the Idaho National Laboratory (INL) and the Technical Director of the INL Wireless Security Institute. The focus of his research is on secure implementation of future generations of wireless communications with scientific exploration and engineering innovations across the fields of wireless technology, cybersecurity, and computational science. Specific goals are to lead and focus wireless security research efforts for 5G and Beyond with national impact, to secure communications for a nationwide unmanned aerial system and for 5G spectrum sharing with distributed scheduling. Arup has extensive industry experience in wireless communications from his work before he joined INL in October 2015. He received his Ph.D. in Engineering and Applied Sciences from Yale University. He is a senior member of IEEE.